NASA/CR—1999-209161

Low-Energy Sputtering Research

P.K. Ray and V. Shutthanandan
Tuskegee University, Tuskegee, Alabama

National Aeronautics and
Space Administration

Glenn Research Center

June 1999

Available from

TABLE OF CONTENTS

LIST OF FIGURES

LIST OF TABLE

1. INTRODUCTION

NASA's Solar Electric Propulsion Technology Application Readiness (NSTAR) program has baselined the 30-cm xenon ion engine technology developed under the On-Board Propulsion (OBP) program. The NSTAR system is a prime candidate for application in early planetary missions being proposed to NASA's New Millennium initiative [1]. Flight qualification of an ion thruster requires a demonstrated life time of 5000 to 10000 hours or more. The principle life-limiting element in an ion propulsion system is the thruster ion optics [2].

Specifically, the two grid optics undergo two different sputtering processes. The accelerator grid biased negatively with respect to the discharge chamber, is subject to the impact of charge exchange ions produced just downstream of the grid [3]. They impinge on the downstream side of the grid with energies of approximately 200 eV. This effect is due to the higher than desired pressure in the test facilities. The positive grid is bombarded on the upstream side by low energy ions in the discharge chamber. The energy of these ions is approximately equal to the discharge voltage (25 V) for a 2.3-KW, 30-cm xenon thruster. It has been determined that practically all of the sputter erosion is due to the doubly charged ions peaked at the center of the thruster. The energy of the doubly charged ions is assumed to be twice the energy of the singly charged ions.

It has been observed that the energies of ions produced near a hollow cathode can be several times the anode-to-cathode potential difference [4]. The sputtered materials from these ion-surface interactions are deposited on to adjacent structures inside the discharge chamber. Subsequent formation of flakes when the sputtered materials of sufficient thickness peel off from these structures is also a major concern [5-7].

Sputtering yields have been measured at low ion energies for various metal-ion combinations. However, there are uncertainties about the low-energy yield data, particularly below 200 eV. With a variety of surface conditions of the targets and the experimental techniques involved, it is not surprising that sputtering yield data reported by different authors show considerable variations.

Three methods have been tried successfully to measure sputtering yields at low ion energies:

1. Weight loss method [8.9]

2. Optical spectroscopy method [10]

3. Radioactive tracer method [11-13]

However, each method has its disadvantages. The weight loss method has been used extensively but this method requires a high ion current density to provide a measurable weight loss in a relatively short time. Hence, for low-energy sputtering measurements, using the weight loss method, experiments were performed in plasma discharge systems. The optical spectroscopic method is also applicable in plasma discharge experiments. A general disadvantage of the plasma discharge systems is that the irradiation conditions are somewhat poorly defined and impurities in the plasma could contribute to the measured yields. Moreover, at ion energies near the sputtering threshold, different charge states of the ions could provide erroneous values of the sputtering yields.

The radioactive tracer method has been found to be highly sensitive, even near threshold energies. The disadvantage of the radioactive tracer method is that only a few suitable radioisotopes are available as tracers. For example, accelerator grids are made of molybdenum which do not have a suitable radioisotope.

This prompted us to search for experimental techniques which can be used to measure small amount of sputtered atoms. Two methods appear to be applicable in our situation. One is Rutherford backscattering spectrometry (RBS). In this method, sputtered material is deposited on a foil and the amount of deposited material is measured by RBS. The RBS technique can measure reliably as little as one monolayer of deposited material. The RBS method has been used in high-energy sputtering measurements [14-16], but it has not been used in low-energy sputtering studies presumably due to the large amount of time required to deposit a measurable amount of sputtered material on the collector foil.

Sputtering yields can also be measured by secondary neutral mass spectrometry (SNMS). When a primary ion strikes a solid surface, it induces a series of elastic collisions in the near surface region of the target. At low ion energies, a fraction of the primary ion energy may occasionally be consumed in the ejection of some atomic particles from the surface. A majority

(> 99 % for metals and alloys) of these sputtered particles is neutral. Hence, a mass spectrometric analysis of these sputtered neutrals can be used as measure of the sputtering yields.

In view of this, an experimental study has been initiated at Tuskegee University to measure low-energy sputtering yields from molybdenum with xenon ions using both RBS and SNMS methods. The objective of this research was to set up an experimental assembly to bombard materials with low-energy ions and obtain sputtering yield data under well-defined experimental conditions. In this report, we present the results of the first part of our study involving the sputtering of molybdenum with xenon ions having energies between 150 and 600 eV.

While performing these experiments, we observed that heavy isotopes are sputtered preferentially over light isotopes at low energies when xenon is used as the primary ion. This is contrary to the usual observation of preferential light isotope emission in the sputtering process. We have investigated this aspect of preferential sputtering by bombarding copper with xenon ions with energies ranging from 150 eV to 1.5 keV. The results are also presented in this report.

2. EXPERIMENTAL SET-UP

The major components of the experimental system and some operating parameters are described below.

2.1 Vacuum system

The experiments were performed inside a spherical vacuum chamber. The diameter of the chamber was 22.5 cm. A 170 liter/sec, 2-stage turbomolecular pumping system was used to provide the required vacuum conditions. The pump can attain a base pressure in the region of 1×10^{-9} Torr inside the chamber. The pressure inside the chamber was monitored by a hot cathode ionization gage. A gate valve was incorporated between the vacuum chamber and the turbomolecular pump to isolate the pump from the vacuum chamber as needed.

2.2 Ion gun assembly

An ion gun was used in the present investigation. The ion gun has the capability of generating noble gas ions such as xenon and argon in the energy range 10 eV to 3 keV. The gas enters the ion gun through a port multiplexer. Xenon gas of 99.999% purity was used in our experiments. A uniform ion beam current was maintained by a stabilized gas flow system. When xenon was introduced into the vacuum chamber, the pressure increased to 1×10^{-6} Torr.

The ion gun can deliver a beam current of 0.005 μA at 10 eV and 0.35μA at 500 eV. The ion beam can be focused on a target at a distance of 20 mm from the exit plane. The size of the focused beam is approximately 1 mm in diameter. A Raster Generator Deflection Unit was used to move the beam on the target surface. This unit is capable of rastering the beam both along the x- and the y- axes in a 4 mm x 4 mm area.

The ion current was measured by a Faraday cup which was mounted on the ion gun. It could be actuated pneumatically to intercept the ion beam at a distance of 6 mm from the exit

plane of the ion gun. The Faraday cup was interfaced with an electrometer to provide the ion current reading.

2.3   Rutherford backscattering spectrometer

One MeV helium ions were used for the RBS measurements. The helium ions were generated from a 2 MV Van de Graaff accelerator which is connected to the RBS chamber via a differentially pumped beam line. The helium ions are separated from the impurities by using the bending magnet to steer ions with the correct e/m ratio into the beam line. All measurements were performed at a pressure of 1×10^{-8} Torr.

The sample (sputtered Mo deposited on an Al strip) is mounted on a specially designed sample holder. This assembly is then attached on to a three-axis goniometer. The sample holder consists of a tantalum plate, aluminum plate and a current measuring device. The tantalum plate is electrically isolated from the sample holder by three ceramic washers so that the helium beam current striking the sample can be measured.

The backscattered ions are energy analyzed and counted using a planar silicon detector. The detector is mounted 3 inches from the sample, and is positioned at a scattering angle of 155°. The angular spread of the beam at the detector is reduced by mounting a small circular aperture in front of the detector.

The helium beam current was measured by integrating the sample current over the data collection time. Typically 3 micro-coulombs of charge was used in each run.

2.4   Secondary neutral mass spectrometer

A mass spectrometer was used to measure sputtering yields of molybdenum at low ion energies. The spectrometer has the capability of operating in the following modes: (i) secondary neutral mass spectrometry (SNMS), (ii) secondary ion mass spectrometry (SIMS), (iii) residual gas analysis (RGA), and (iv) thermal desorption mass spectrometry. The major components of the spectrometer is depicted schematically in Fig. 1.
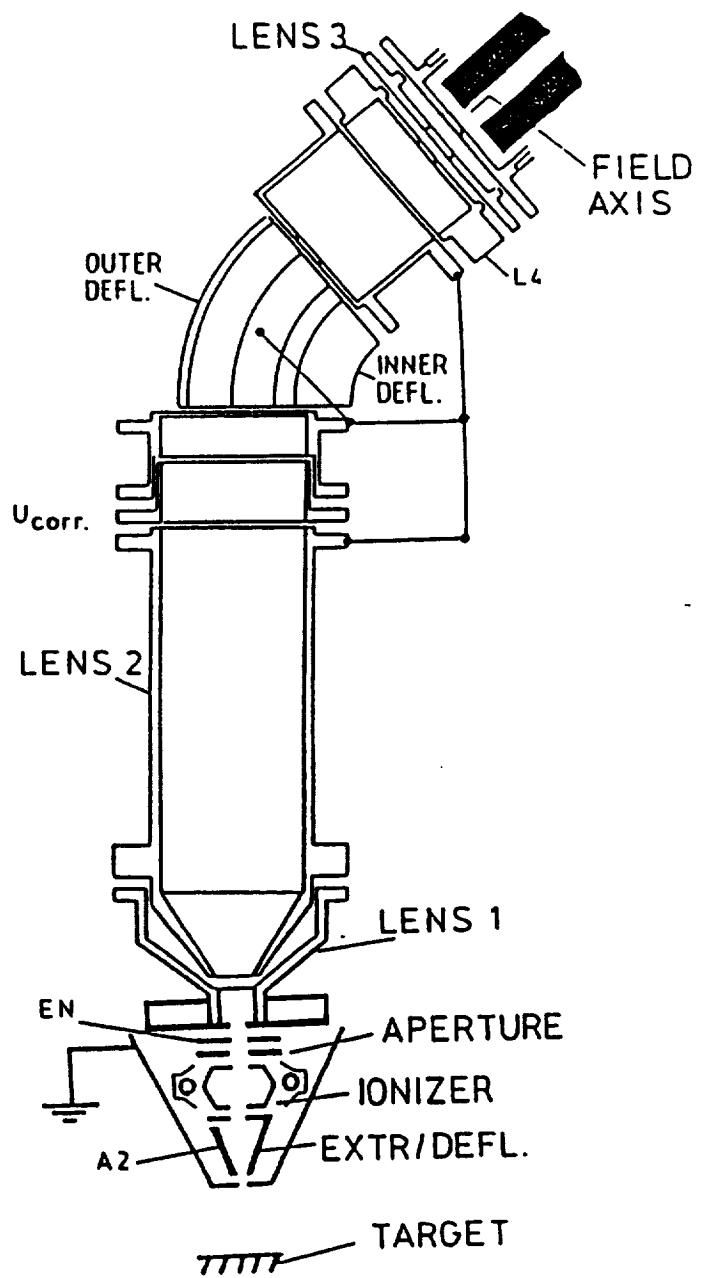
Fig.1. Schematic diagram of the mass spectrometer

In the SNMS mode of operation, the sputtered neutrals are ionized by electron impact in a region defined by the ionizer inside the spectrometer. The ionization of the sputtered neutrals was performed by a 5 mA electron beam at 50 eV. The residual gas particles which are also ionized possess kinetic energies in the 0.001 to 0.1 eV range and are prevented from entering the mass filter by applying an appropriate retarding electric field. The postionized neutrals, which have energy in the 1 to 10 eV range, are subsequently mass analyzed by a quadrupole system and detected by a single channel electron multiplier. During the operation of the spectrometer in the SNMS mode, positive secondary ions are electrostatically deflected before they can reach the ionizer volume and negative secondary ions are removed by the optical system since all functional elements are set to transport positive ions only. The spectrometer can effectively collect and separate secondary ions, postionized neutrals and residual gas signals from each other at a very high dynamic ratio.

Two lenses (LENS 1 and LENS 2) are used to focus the ionized particles from the ionizer volume to the front of the energy analyzer. An electrostatic energy filter serves to transport ionized neutrals to a third lens (LENS 3) and filter out all uncharged particles coming from the ionizer region. The energy analyzer also suppresses a majority of ionized residual gas molecules that are not blocked by the retarding field. The focusing of charged particles leaving the energy filter into the quadrupole mass filter is controlled by LENS 3. The transfer lens (L 4) operates as an accelerating immersion lens and focuses the charged particles into the quadrupole rod system.

The high transmission quadrupole system with a mass range of 0-511 amu is controlled by the data acquisition unit connected to a computer. The mass filter consists of four cylindrical rods arranged symmetrically to the z-axis. Each pair of opposite rods in connected between two pairs of rf voltage with superimposed dc voltage. The ions injected into the mass filter in z direction are stimulated by electric field to oscillate in x and y direction. The proper selection of voltages enables ions of a particular e/m ratio to emerge out of the system for detection by a secondary electron multiplier capable of handling count rates in excess of 5×10^6 cps. The

output pulses of the electron multiplier. after further amplification and discrimination. are fed to a computer for data evaluation and storage.

2.5   Effect of residual gases

It is well known that the presence of background gases has the effect of lowering the values of the measured sputtering yields. Nitrogen. for example. is easily chemisorbed on Mo and it will act as a buffer to the impinging ions. thus reducing the measured sputtering yields. To ensure that a dynamically clean sputtering condition exists, one can use the following criterion[20]:

$$\frac{Y_{i,s} I}{f \beta_{i,s}} \geq 10 \tag{1}$$

where $Y_{i,s}$ is the sputtering yield of species i, I is the ion flux impinging on target s, f is the background gas flux impinging on target s, and $\beta_{i,s}$ is the sticking probability of background gas species on target s.

To calculate the ratio defined by Eq. (1), it is assumed that the bulk of the chemisorbed gas on the target surface is nitrogen. The sputtering yields of chemisorbed nitrogen were calculated using the formulation developed by Winters [17]. At 200 eV, the sputtering yield of nitrogen for xenon ions is 0.2 atom/ion. The sticking coefficient is assumed to be equal to one because of the high reactivity of the species in the presence of the ion beam. For our experimental conditions, the ratio defined by Eq. (1) is estimated to be over 50 which is much higher than the recommended value of 10. Therefore, no reduction of the sputtering yield of Mo due to background gases is expected in our measurements.

3. MEASUREMENT OF SPUTTERING YIELD BY RUTHERFORD BACKSCATTERING SPECTROMETRY

3.1   Introduction

The RBS technique is a non-destructive surface analysis method where an energetic light ion beam is directed at the surface of the sample. The ions interact with atoms in the sample and some of them are backscattered into a detector. From the energy spectrum of backscattered ions one can infer considerable information about the sample's thickness and composition [18].

3.2   Theory

A typical RBS spectrum from a thin film deposited on a single element substrate is shown in Fig. 2, where an ion beam with energy E_0 strikes the sample at normal incidence and backscattered ions are detected at a scattering angle θ. When thin films of high atomic numbers are deposited on a substrate of low atomic number, the peak and the continuum of the backscattered spectrum are well separated. The ions scattered from the surface atoms of the thin film will reach the detector with energy KE_0 (K<1) where K is given by the following equation:

$$K = \left\{ \frac{\left[\left(M_2^2 - M_1^2 \sin^2 \theta \right)^{1/2} + M_1 \cos\theta \right]}{M_1 + M_2} \right\}^2 \tag{2}$$

Here, θ is the scattering angle, M_1 is the mass of the incident ion, and M_2 is the mass of the target atom.

The ions scattered from the atoms which are below the surface will give signals at energies less than KE_0, as shown in Fig. 2. The backscattered ion yield, A, from a thin film deposited on a light material substrate is given by,

$$A = QNt \left(\frac{d\sigma}{d\Omega} \right)_{film} \Omega \tag{3}$$
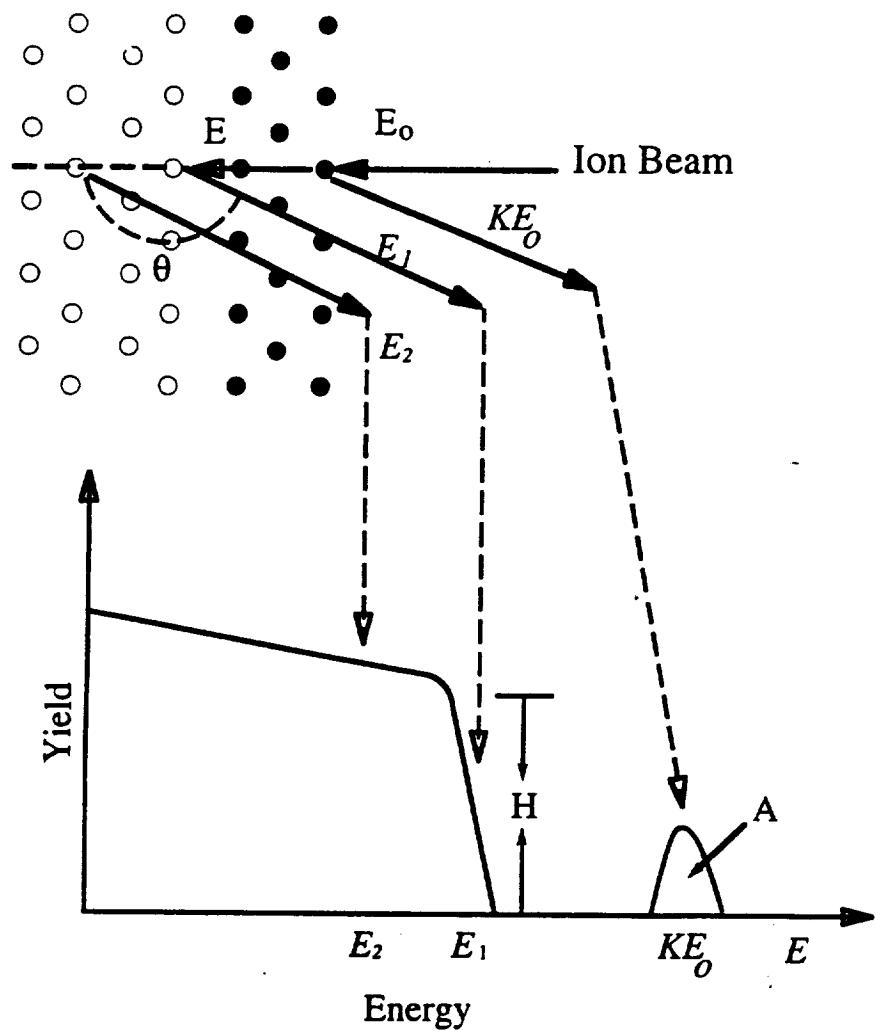
Fig. 2. Schematic diagram depicting the RBS technique

where, Q is the number of incident helium ions at the target. N is the atomic density (atoms/cm^3), t is the thickness of the sputtered film. $d\sigma/d\Omega$ is the differential Rutherford scattering cross-section, and Ω is the solid angle subtended by the detector relative to the helium beam spot on the sample surface.

The backscattering yield in the surface region is equal to the area under the peak and this can be measured from the backscattered data. The parameter $d\sigma/d\Omega$ is calculated from the following equation:

$$\frac{d\sigma}{d\Omega} = F\left(\frac{z_1 z_2 e^2}{2E_o \sin^2\theta}\right)^2 \frac{\left\{\left[1-\left(\frac{M_1 \sin\theta}{M_2}\right)^2\right]^{\frac{1}{2}} + \cos\theta\right\}^2}{\left[1-\left(\frac{M_1 \sin\theta}{M_2}\right)^2\right]^{\frac{1}{2}}} \tag{4}$$

where F is a screening correction factor and is given by

$$F = 1 - \frac{0.042 z_1 z_2^{4/3}}{E_o} \tag{5}$$

and E_o is the energy of the incident helium ions in keV.

The backscattering yield from the surface of the substrate is proportional to the edge height, H, which is given by,

$$H = \frac{\Delta E}{\left[\varepsilon_o\right]} Q\left(\frac{d\sigma}{d\Omega}\right)_{Substrate} \Omega \tag{6}$$

where H is the edge height of the RBS spectrum, ΔE the width of a single channel of the spectrum, and [ε_o] is given by the following equation:

$$[\varepsilon_o] = K\varepsilon(E_o) + \frac{\varepsilon(KE_o)}{\cos\theta} \qquad (7)$$

where ε is the stopping cross section [18].

From equations (3) and (6) the value of Nt is obtained as

$$Nt = \frac{A}{H}\frac{\Delta E}{[\varepsilon_0]}\frac{\left(\dfrac{d\sigma}{d\Omega}\right)_{substrate}}{\left(\dfrac{d\sigma}{d\Omega}\right)_{film}} \qquad (8)$$

Thus the edge height (H) and the peak area (A) of the backscattered spectrum provide the Nt values.

We are interested in determining the differential sputtering yield $Y(\theta)$ which is defined as the number of sputtered atoms per incident ion per unit solid angle. Once the Nt values are obtained, $Y(\theta)$ can be calculated from the following equation:

$$Y(\theta) = \frac{R^2 Nt(\theta)q}{IT} \qquad (9)$$

where R is the radius of the collector strip, q is 1.6×10^{-19} C/ion, I is the xenon beam current, and T is the total sputter time.

3.3   Experimental procedure

The target was mounted on a $XYZ\theta$ manipulator for precise positioning within the vacuum chamber. During sputtering, the target was placed at a distance of 20 mm from the exit plane of the ion gun. At this position, the ion beam could be focused to a spot approximately 1 mm in diameter. The target was bombarded by xenon ions at 200 and 500 eV at normal incidence, and the sputtered Mo atoms were collected on a thin, semi-circular collector foil as shown in Fig. 3. The foil was mounted on a 12.5 mm wide collector plate which formed a semi-

circle of 15 mm radius around the position where the ion beam was focused on the target (Fig. 3). A 5 mm diameter hole in the center of the collector plate and the Al foil allowed the passage of the ion beam.

To determine if the surface condition of the target had any measurable effect on the sputtering yield, two different targets were used. Both targets were 12.5 mm in diameter and 6.2 mm in thickness and were cut from a rod of 99.5% purity. One of the targets was unpolished but cleaned with acetone and distilled water and the other target was electropolished.

All RBS measurements except one were performed at Montana State University (MSU). The sputter deposits from the electropolished sample were analyzed using the RBS facility at the Pacific Northwest National Laboratory (PNNL). In both cases, 1 MeV helium ions were used to probe the collector foil. The backscattered ions were detected by a solid-state detector located at 155^{0} (MSU) and 165^{0} (PNNL) to the direction of the helium ion beam. From the RBS data, the quantity Nt is determined as a function of ejection angle. The diameter of the He ion beam was 2 mm and hence the points where the measurements were made were 2 mm apart. Figure 4 shows the shape of the foil and points where the measurements were made.

3.4   Data analysis

In the case of high-energy sputtering (ion energies in the keV region), the sputtered atoms are observed to follow a cosine angular distribution [19]. Thus, the function $A\cos^{n}\theta$ is generally used to fit the high-energy differential sputtering yield data. However, in low-energy sputtering, the angular distribution of the sputtered particles has been observed to be under-cosine [20]. In order to retain the cosine character of the angular distribution, the differential sputtering yields obtained from Eq. (9) were fitted using the following function:

$$f(\theta) = A_1 \cos\theta + A_2 \cos^2 \theta + A_3 \cos^3 \theta + A_4 \cos^4 \theta \tag{10}$$

The total sputtering yield is obtained by integrating $f(\theta)$ with respect to the solid angle:

13
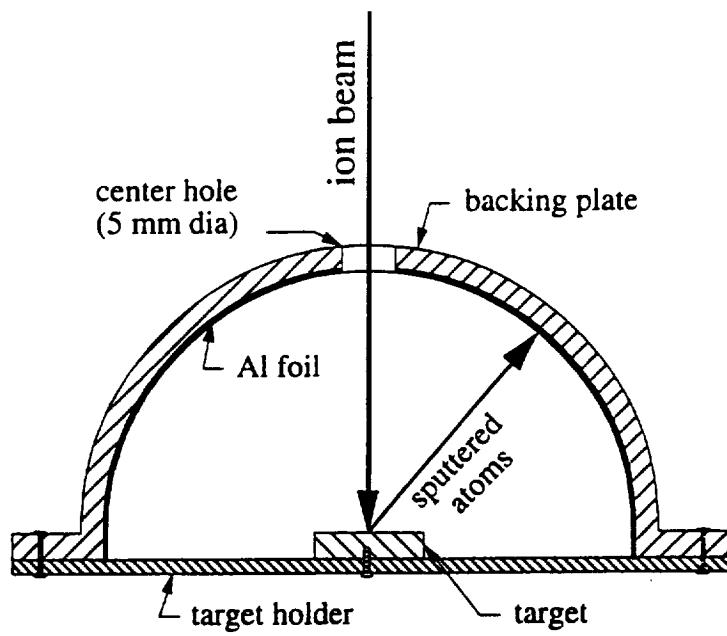
Fig. 3. Schematic diagram of the target-collector assembly
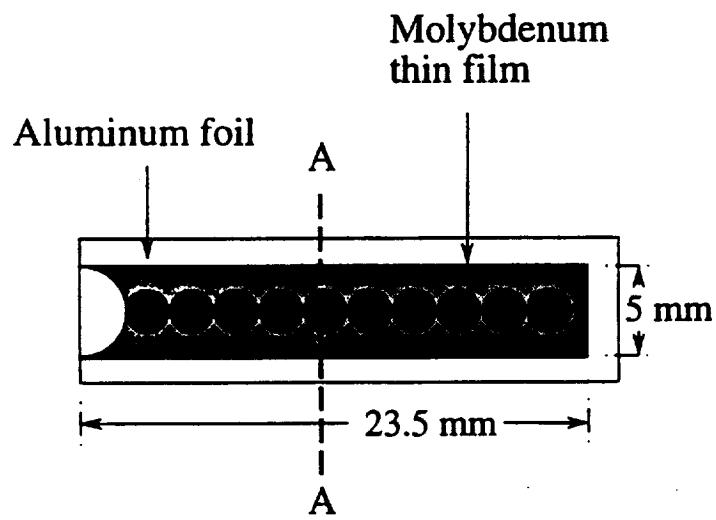
Fig. 4. Location of RBS measurements on the collector foil.

$$Y_{tot} = \int f(\theta) 2\pi Sin\theta d\theta$$

$$= 2\pi(\frac{A_1}{2} + \frac{A_2}{3} + \frac{A_3}{4} + \frac{A_4}{5})$$ (11)

3.5   Results and Discussion

One of the uncertainties in RBS measurements is the sticking coefficient of the sputtered particles on the substrate when the first monolayer is formed. Three different substrates were used in sputtering with 500 eV xenon ions to determine the substrate to which the sputtered particles adhere best. The substrates tested were plain aluminum foil, plasma etched aluminum foil and grafoil. It was found that among the three substrates tested, the sticking probability of sputtered Mo is highest on the plain aluminum foil and lowest on grafoil. Hence, all subsequent depositions were made on plain aluminum foils. In our RBS calculations, the sticking coefficient has been assumed to be one.

Sputter depositions from the unpolished target were made at both 200 and 500 eV whereas the electropolished target was sputtered only at 200 eV. All sputtering was done at normal incidence. For the 200 eV run, the plain target was bombarded for 50 hours while the electropolished target was sputtered for 34 hours. For the 500 eV run, the plain target was sputtered for 30 hours. The ion gun was run 8 to 10 hours each day to collect data.

To determine the uniformity of deposition across the width of each substrate, RBS measurements were first performed at around 45^0 target emission angle along line A-A (Fig. 4). The resulting Mo peak areas obtained from the unpolished sample are plotted in Fig. 5 for 200 and 500 eV incident ion energies. It can be seen from this figure that maximum Mo counts are obtained from the central portion of the collector foil. This region also happens to be larger than the helium beam diameter. The center of this region was determined in each run and along that line all subsequent RBS measurements were performed.

The RBS measurements indicated that measurable amounts of sputtered material were deposited on all runs. The least amount of deposit was in excess of one monolayer at 82^0 target emission angle at 200 eV. Figure 6 shows a typical RBS spectrum taken at 200 eV at 44^0

15
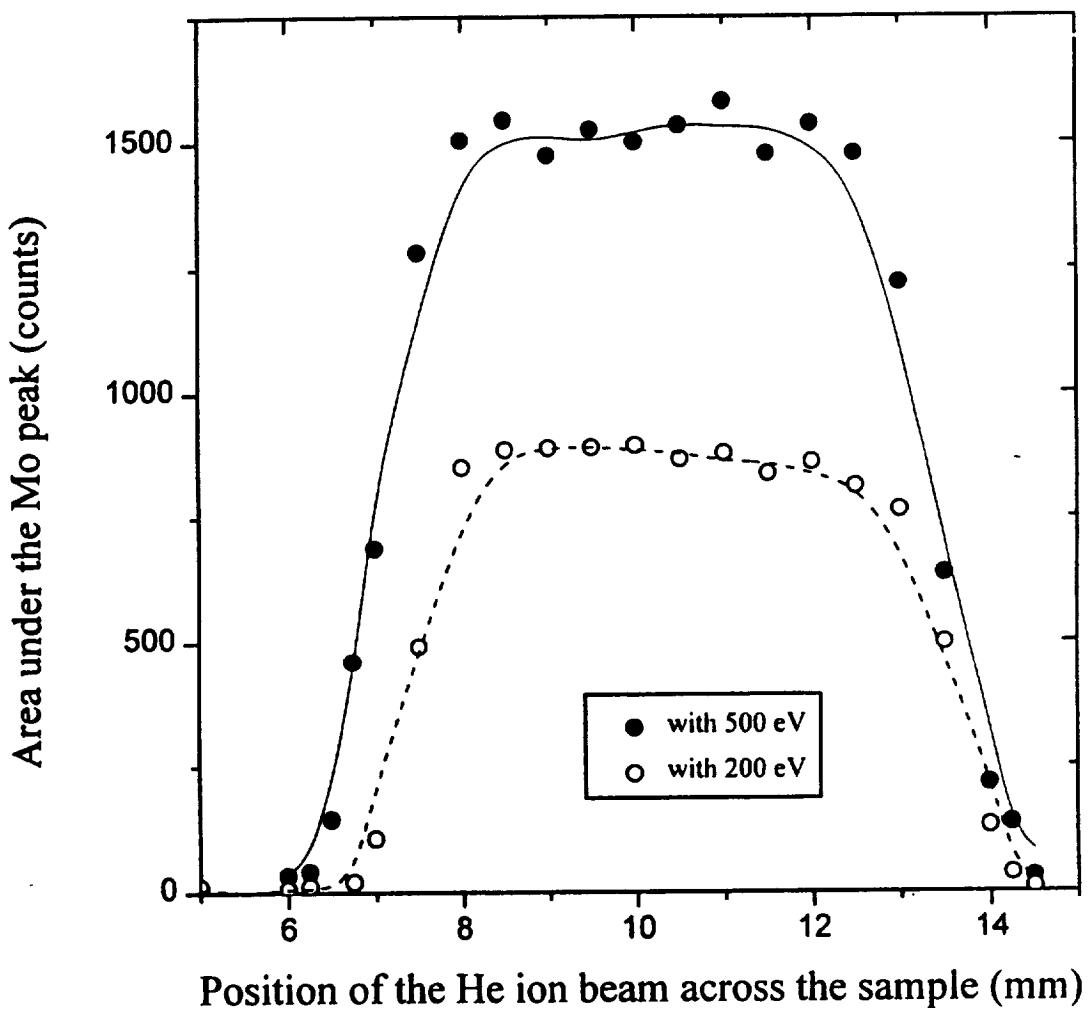
Fig. 5. Mo peak area as a function of He beam position across the foil at A-A
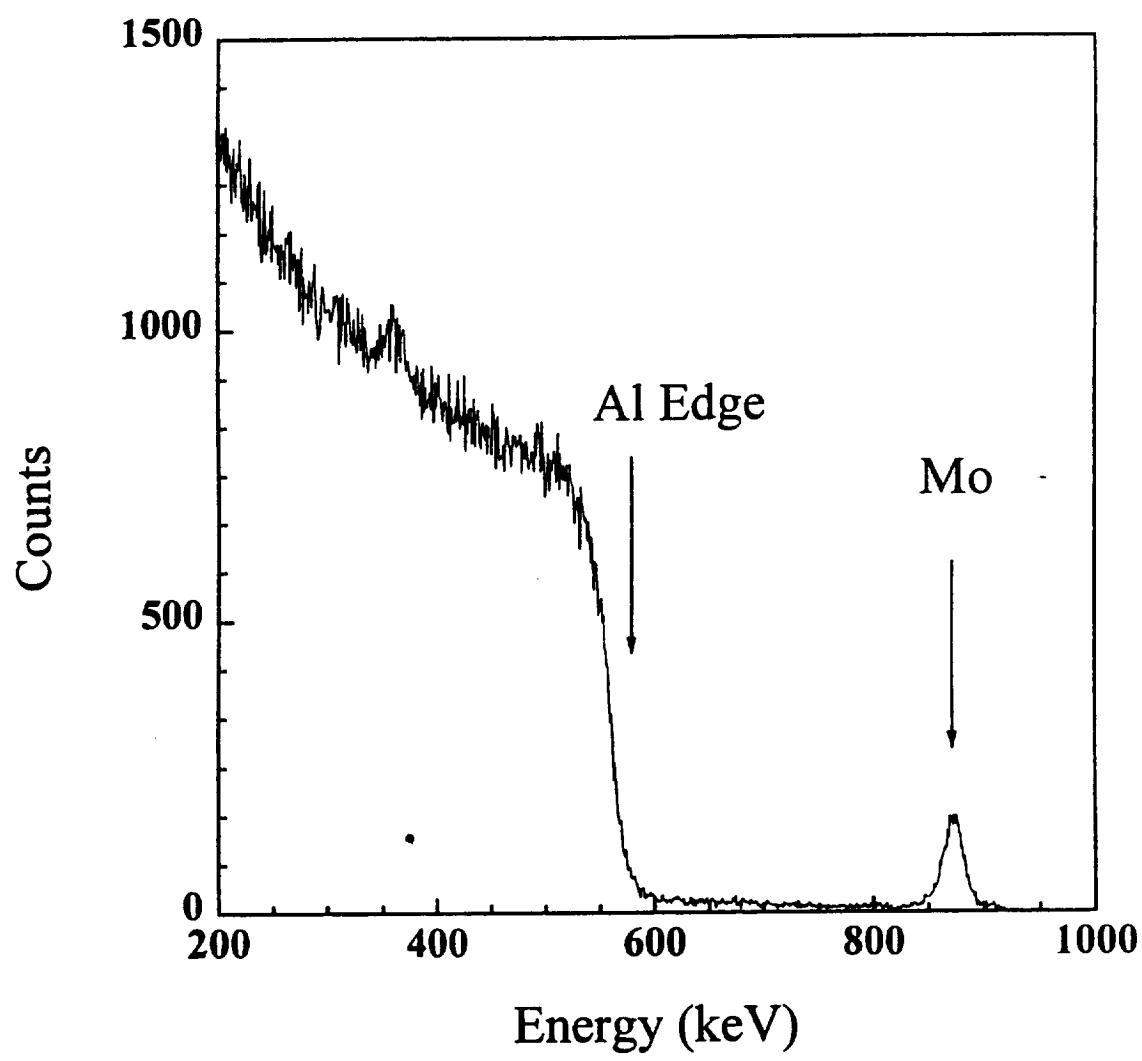
Fig.6. A typical RBS spectrum from Mo deposited on Al foil

target emission angle. At this point, the thickness of the sputtered Mo was in excess of 6 monolayers. The Mo peak was well separated from the substrate backscattering continuum.

The polar plots of the differential sputtering yields obtained from RBS measurements from the unpolished target at 200 and 500 eV are presented in Fig. 7. It is apparent from this figure that the angular distributions of ejected particles are under-cosine. It is also observed that the maximum of this distribution shifts towards larger angles at lower incident ion energies. For example, at 500 eV the maximum occurs at around 45^0 whereas at 200 eV it is around 60^0. The differential yields obtained for these two runs are also shown in Fig. 8 as a function of angle in Cartesian coordinates. They were fitted with the function described in Eq. (10) and integrated over all solid angles to provide total sputtering yields.

The sputtering yields at 200 and 500 eV are presented in Fig. 9. In this figure, low-energy Mo sputtering data of Rosenberg and Wehner [8] and of Weijsenfeld et al [9] are also plotted for comparison. In both of these measurements, spherical targets were immersed in a low-pressure, high-density plasma and sputtering yields were determined from the weight loss of the target The yields obtained by RBS measurements fall in the range of yields measured by these two groups of researchers. In a more recent experiment, thin films of molybdenum were sputtered by ions of xenon and other noble gases [21]. In the low-energy end, with xenon ions, sputtering yields were found to be 0.8 at 200 eV and 1.6 at 500 eV. Since, these values are considerably higher than those obtained by other researchers, these values are not shown in Fig. 9.

The sputtering yields measured by Rosenberg and Wehner are found to be consistently higher (17% at 600 eV and 62.5% at 100 eV) than those obtained by Weijsenfield et al. The yieldmeasured by the RBS method at 500 eV agrees with Weijsenfield's data but at 200 eV they are lower by 27% for the unpolished sample and 14% for the electropolished sample. The fact that the electropolished sample provides a slightly higher yield compared to the unpolished sample indicates that in sputtering yield measurements surface preparation plays some role.

Two factors may influence the sputtering yield measurements using the RBS method. The first one is the sticking coefficient. In this calculation, the sticking coefficient of sputtered Mo atom on the Al foil has been taken as one. However, the sticking coefficient may be less than one when the first monolayer is being formed. Since, the measurement involves only a few
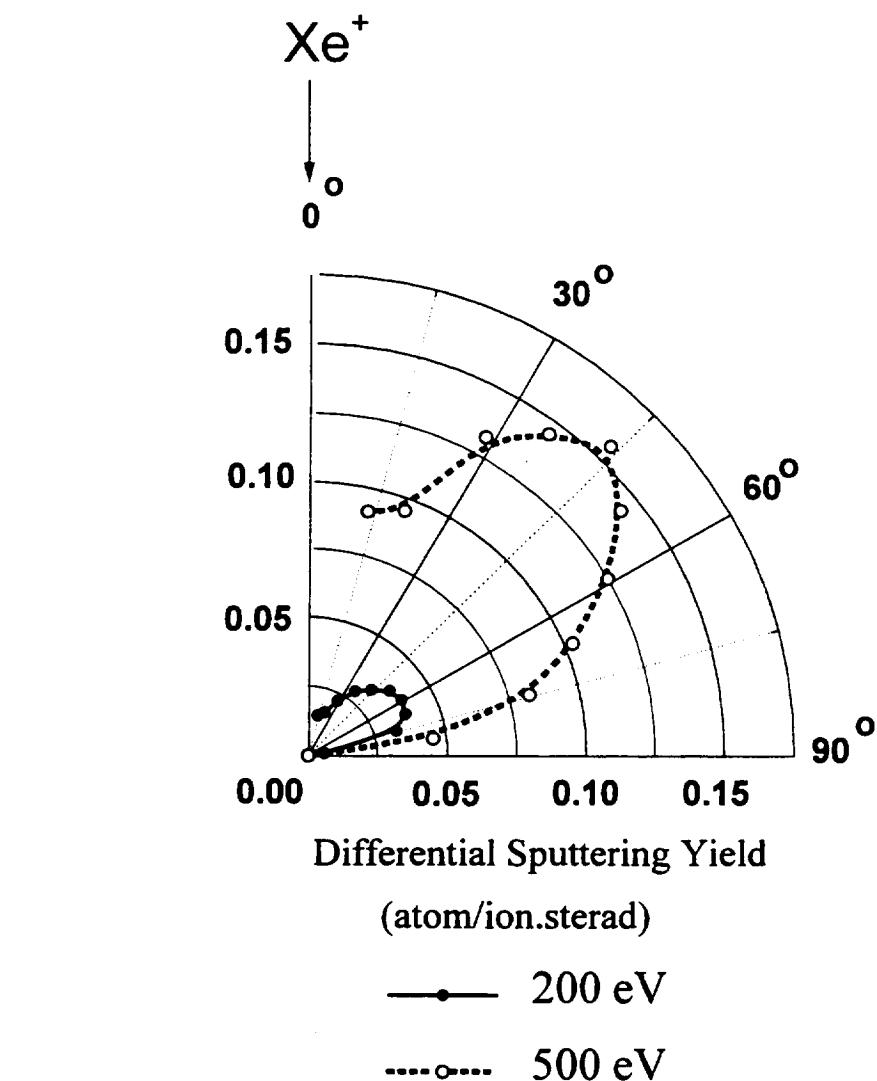
Fig.7. Polar plot of the differential sputtering yield of Mo at 200 and 500 eV
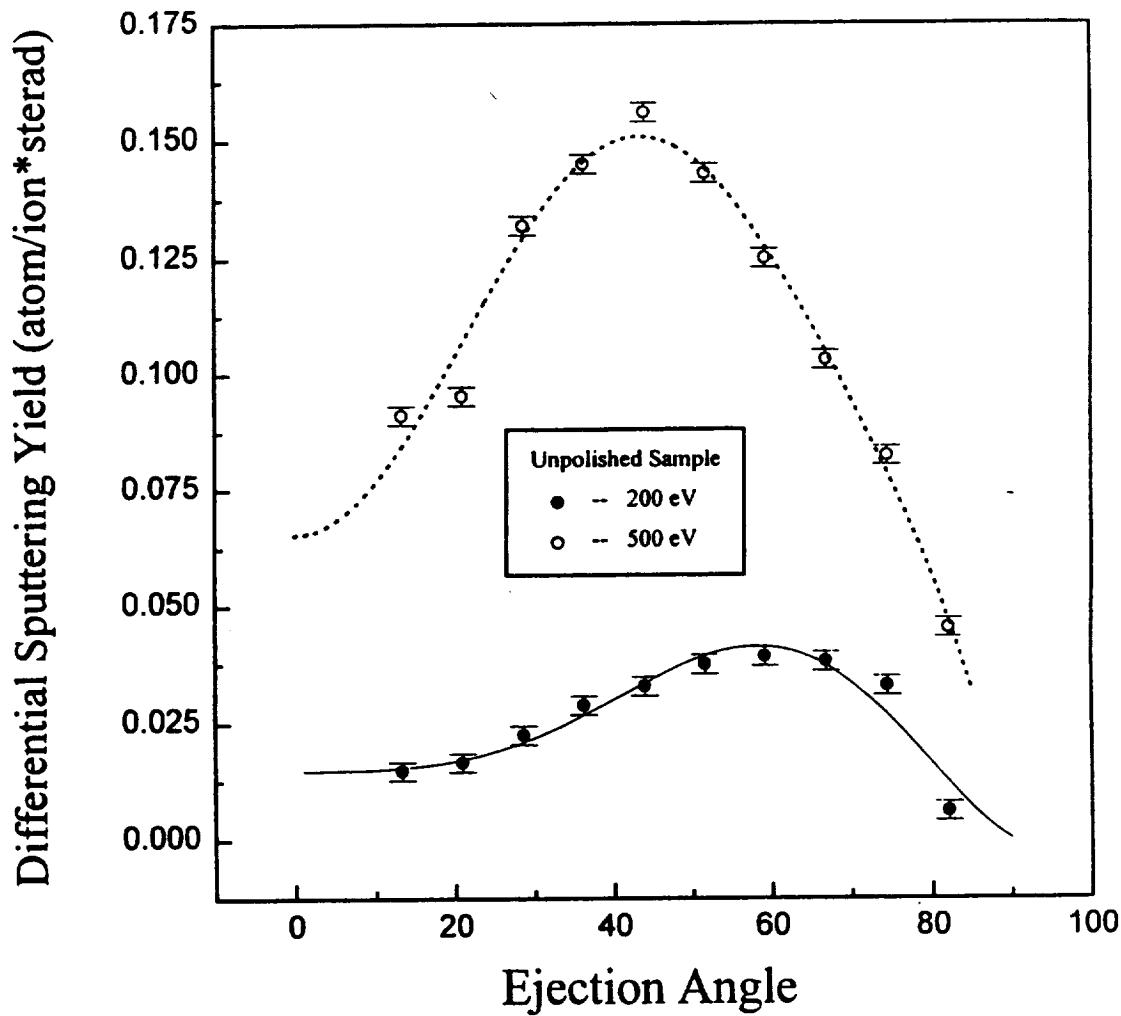
Fig.8. Differential sputtering yield of Mo in Cartesian coordinates at 200 and 500 eV
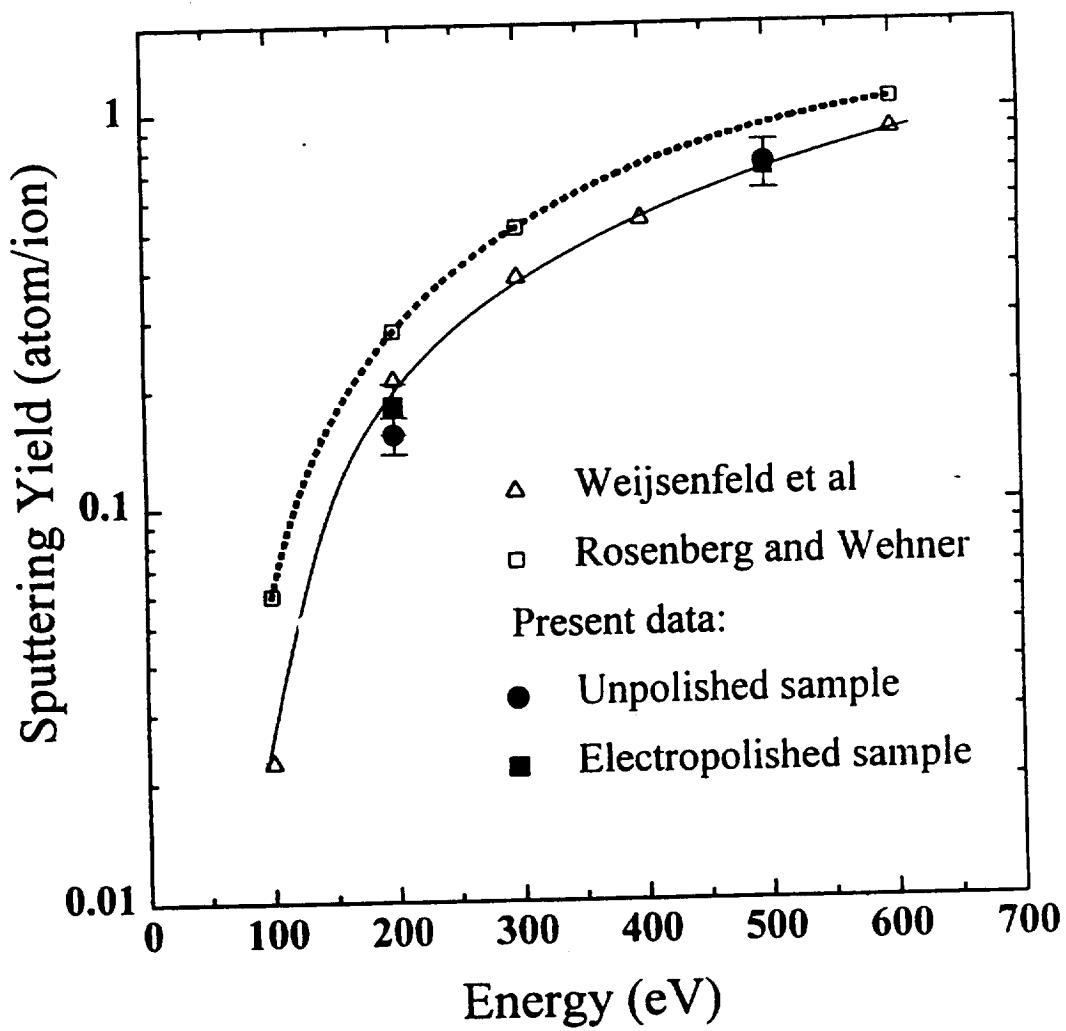
Fig.9. Total sputtering yield of Mo at 200 and 500 eV

monolayers at the most. this introduces some error in the calculation and the actual sputtering yields should be somewhat higher than what is reported here.

The other factor is the assumption that the angular distribution of the sputtered particles is isotropic. This assumption may not be quite accurate. Polycrystalline metal targets have preferred orientation and atoms sputtered from several targets have been observed to be preferentially ejected in the closed-packed direction [22]. If this is true for Mo. the integration of the measured differential sputtering yields over all solid angles would introduce some error.

3.6   Conclusions

Sputtering yields of Mo by xenon ions at 200 eV and 500 eV at normal incidence have been measured using the RBS method. An ion gun was used to produce xenon ions. The values of sputtering yields obtained in this manner are in the range of those measured by other researchers using different techniques. Thus, the RBS method can be successfully used in low-energy sputtering measurements.

Two issues need to be addressed in any future work in low-energy sputtering yield measurements using the RBS method. One is the sticking coefficient of sputtered atoms on the substrate as the first monolayer is formed. The other is the assumption of isotropic angular emission of sputtered particles in the hemispherical space where these particles are ejected.

4. MEASUREMENT OF SPUTTERING YIELD BY SECONDARY NEUTRAL MASS SPECTROMETRY

4.1. Introduction

In the SNMS technique, some of the sputtered neutral atoms are collected by the spectrometer and a fraction of them is ionized by electron impact [23]. Mass analysis of post ionized sputtered neutrals is achieved by using a quadrpole mass filter and an electron multiplier detector. In the present geometrical arrangement, no data of good statistical quality could be collected below 150 eV. Sputtering yields of molybdenum with xenon ions in the 150 to 600 eV energy range are reported in this report.

4.2. Measurement of SNMS spectra

The experimental set-up is shown schematically in Fig. 10. The aperture of the mass spectrometer intercepts only a small amount of particles sputtered from the sample. The mass spectrometer was positioned such that the axis of its entrance aperture was perpendicular to that of the ion gun. The center of the target was located 10 mm below the spectrometer aperture. In this geometric arrangement, the aperture of the spectrometer subtended a solid angle of 0.03 sr at the center of the target. The target was 6 mm thick. It was cut from a 12.5 mm diameter rod of 99.95% purity. It was screwed onto a sample holder which was mounted on a XYZθ manipulator for precise positioning within the vacuum chamber. During sputtering, the target was placed at a distance of 20 mm from the exit plane of the ion gun and at 50° angle to the surface normal. At this position, the ion beam could be focused to an area approximately 1 mm in diameter. It should be noted that the incident beam is not mass-analyzed.

At the operational pressure of 1×10^{-6} Torr, the beam current remained essentially constant from 150 eV to 600 eV at 0.23 μA. Based on the 1 mm spot diameter, the ion current density at the target was approximately 30 μA/cm^2.

During SNMS measurements, the target was sputter cleaned for about 30 minutes with a rastered ion beam at 2.5 keV.

SNMS/SIMS

Ion Gun

Sample

UHV Chamber

Turbo Pump

Gate Valve
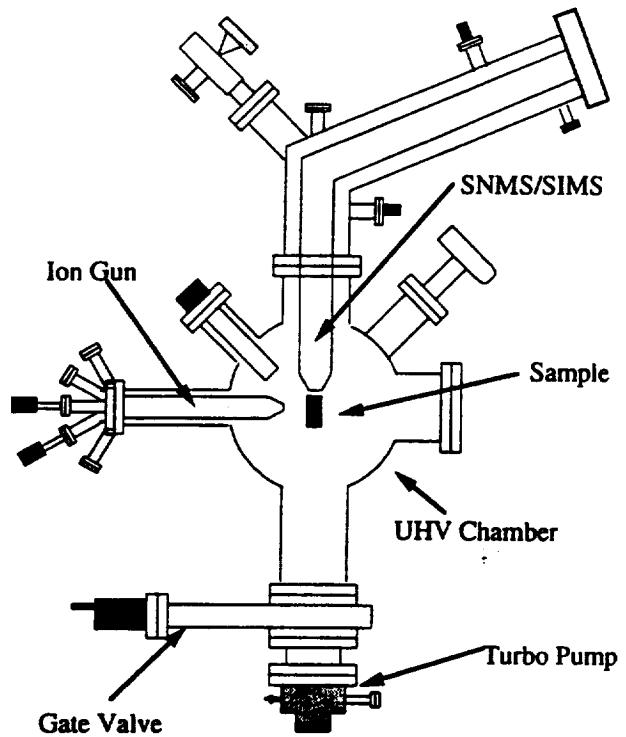
Fig. 10. Scematic diagram of the experimental set-up

24

4.3   Data analysis

The SNMS spectra were measured at an incidence angle of 50°. However, the sputtering yields reported by other researchers were measured at normal incidence. To facilitate comparison of data, the area under the peaks measured at 50° incidence angle in our set-up were converted to sputtering yields at normal incidence. It can be shown that the shape of the yield-energy curve at any angle of incidence is essentially similar to that of the peak area versus energy curve of the SNMS spectra measured at any other angle.

Let $A(\theta, E)$ be the area under the elemental peaks of the SNMS spectra at ion energy E and incidence angle θ. Let the corresponding sputtering yield be $Y(\theta, E)$. Then,

$$Y(\theta,E) = g(\theta,E)A(\theta,E) \qquad (12)$$

where g is a function whose value depends on θ and E. Similarly, the sputtering yield at normal incidence $Y(0°, E)$ is related to the sputtering yield at any other incidence angle by:

$$Y(0°,E) = f(\theta,E)Y(\theta,E) \qquad (13)$$

When a surface is bombarded with low-energy ions, the angular distribution of emitted particles change slightly with energy. The RBS measurements indicate that the peak of the sputtered material distribution shifted from $45°$ to $60°$ when the energy of the primary ions was changed from 500 to 200 eV (Fig. 7). It is assumed in this analysis that in the limited energy range studied (150 to 600 eV), the change in angular distribution of the sputtered materials is not significant. Hence, the functions f and g are assumed to be dependent only on the angle of incidence and not on energy, i.e.,

$$f(\theta,E) \cong f_1(\theta) \text{ and } g(\theta,E) \cong g_1(\theta) \qquad (14)$$

Combining eqs. (12) and (13) with eq. (14), one gets:

$$Y(0^o,E) = f_1(\theta)g_1(\theta)A(\theta,E)$$ (15)

For SNMS spectra collected at a given angle of incidence, ($\theta = 50^0$ in our case), $f_1(50°)g_1(50°) = K = $ constant,. Hence,

$$Y(0'',E) = KA(\theta,E)$$ (16)

Hence, the total sputtering yield at normal incidence is proportional to number of particles sputtered into a small solid angle leading to the entrance of the SNMS aperture. The value of the constant K was determined by normalizing the peak area with the sputtering yield measured by RBS method at 500 eV as described in the previous section.

4.4.   Results and discussion

4.4.1. SNMS spectra

Each spectrometer scan was performed over a 15 s period. At each energy, data were collected using a sweep rate of 2 amu/s and were accumulated over 10 scans at 150 to 600 eV. It is estimated that the maximum target thickness that was sputtered away during SNMS experiments was less than 2 nm.

A full range mass scan revealed the presence of the residual gases as well as small amount of impurities in the target such as Si, Ca, Ti and Zn. The amount of xenon was small indicating effective suppression of residual gas particles by the mass spectrometer energy filters. In spite of raster cleaning the target surface before acquiring the SNMS data, some MoO was always present in the mass spectra.

Typical mass spectra at 150, 200 , and 500 eV are shown in Fig. 11 in the 90 to 120 amu mass range. The Mo spectra at 150 and 200 eV are also shown in the inset in this figure in the 90 to 102 amu mass range. All seven isotopes can be identified in the Mo spectra. Isotopic peaks in these spectra are not well resolved because data were acquired at a relatively low mass resolution to obtain high signal intensities. The intensity of MoO is less than 2.5% of the total intensity at

26
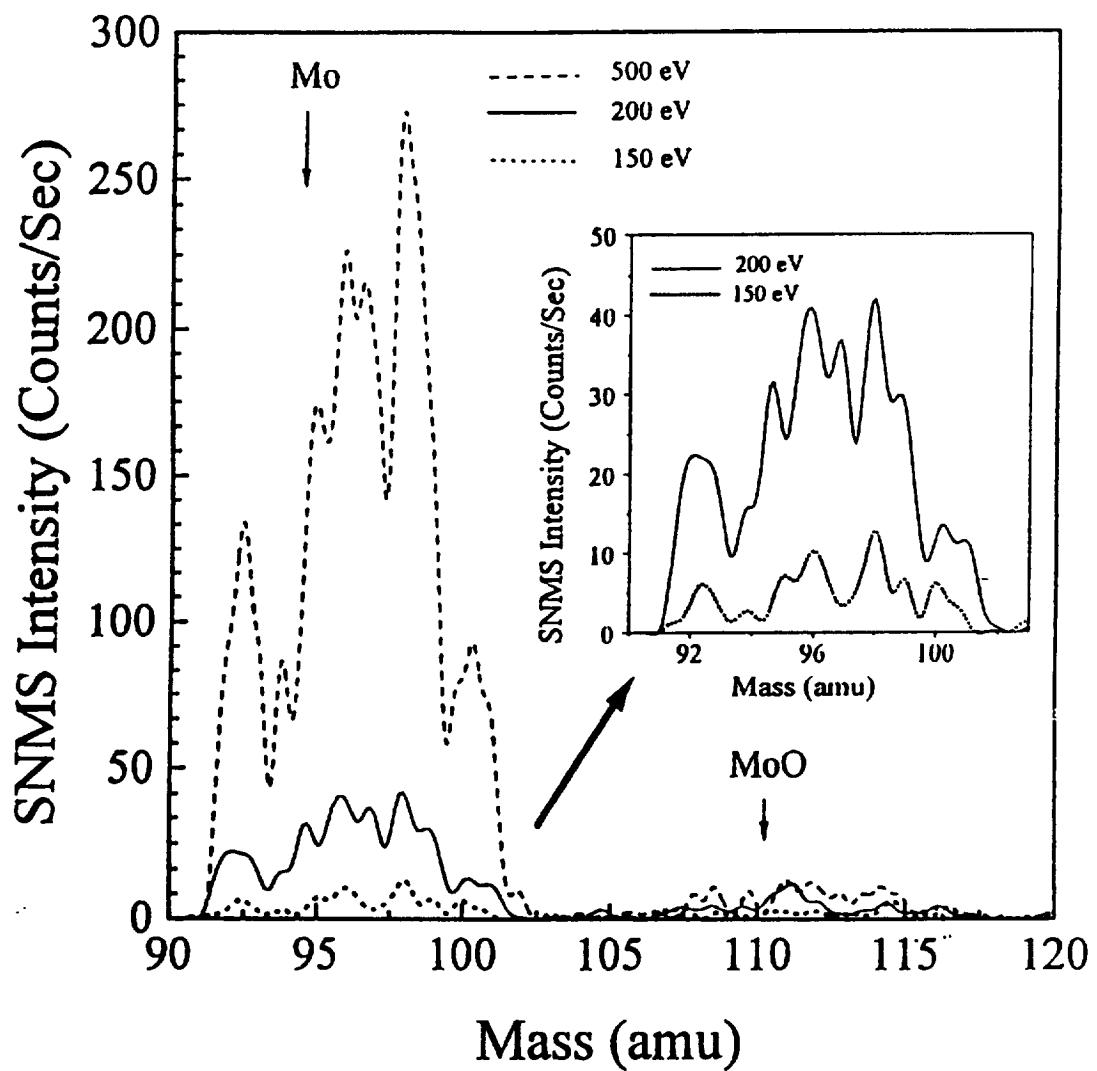
Fig.11. SNMS spectra of Mo by 150, 200 and 500 eV xenon ions

600 eV and increases monotonically to 6.5% of the total intensity at 150 eV. Even though nearly 6 nm of the target surface was removed during raster cleaning of the target, apparently some MoO either remained on the target or was continuously formed on the surface from the bombardment of residual oxygen atoms inside the vacuum chamber. The increase in the percentage of MoO with decreasing ion energy is probably due to the slight displacement of the focus of the ion beam at lower ion energies.

4.4.2 Sputtering yield

In the RBS measurements, both Mo and MoO were counted, as MoO could not be distinguished from Mo by He^+-ion backscattering. Hence, areas under both Mo and MoO peaks were used in converting the SNMS spectra to sputtering yields.

The sputtering yield-energy curve for Mo at normal incidence obtained using the procedure outlined in the previous sections is shown in Fig. 12. For comparison, xenon ion yields of Mo reported by Rosenberg and Wehner [8] and by Weijsenfeld et al [9] are also plotted in the same figure. In both of these measurements, spherical targets were immersed in a low-pressure, high-density plasma and the sputtering yields were determined from the weight loss of the target. It can be seen that the yields obtained by SNMS measurements fall in the range of yields measured by others. However, the shape of the yield-energy curve is observed to be slightly different. Particularly, beyond 300 eV ion energy, the slope of the yield-energy curve is found to be smaller .

4.5   Comparison with theoretical predictions

The most applicable theory of sputtering has been developed by Sigmund [24,25]. This theory predicts good agreement with measured sputtering yields in medium to high energy sputtering cases. It is based on a nuclear energy loss mechanism in which the energy loss is shared among the large number of atoms which define the collision cascade. According to this theory, the sputtering yield Y by ions of energy E at normal incidence is given by the following equation:
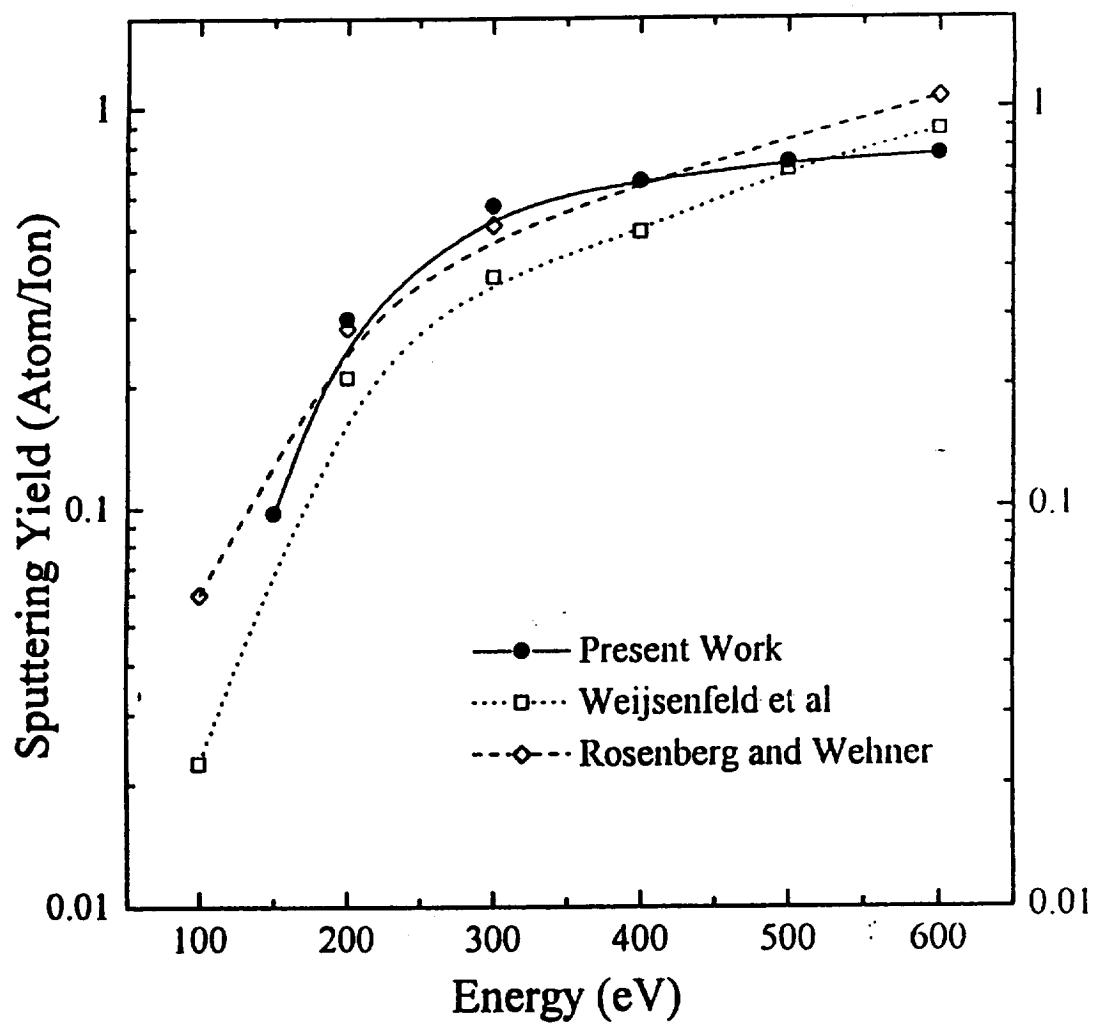
Fig.12. Sputtering yield of Mo as a function of xenon ion energy

$$Y(E) = \frac{0.042}{U_o} \alpha S_n(E) \tag{17}$$

where U_O is the binding energy of the target atoms in eV (for metals the sublimation energy is used), α is a function which depends only on the target atom to ion mass ratio, M_2/M_1, and $S_n(E)$ is the energy dependent nuclear stopping cross section. The value of α is approximated as [21]:

$$\alpha = 0.15 + 0.13 \frac{M_2}{M_1} \tag{18}$$

whereas $S_n(E)$ is described by the following analytical function developed by Lindhard et al [24,26]:

$$S_n(E) = 84.78 \frac{Z_1 Z_2}{(Z_1^{2/3} + Z_2^{2/3})^{1/2}} \left(\frac{M_1}{M_1 + M_2} \right) s_n(\varepsilon) \tag{19}$$

Here $s_n(\varepsilon)$ is the reduced elastic cross-section based on reduced energy ε, and Z_1 and Z_2 are atomic numbers of the ion and target respectively. The value of ε is given by [24,26]:

$$\varepsilon = \frac{0.03255}{Z_1 Z_2 (Z_1^{2/3} + Z_2^{2/3})^{1/2}} \left(\frac{M_2}{M_1 + M_2} \right) E(eV) \tag{20}$$

There are several equations that one can use in describing the function $s_n(\varepsilon)$. Sigmund used an expression based on the Thomas-Fermi model of atomic interaction in comparing the theory with sputtering yield data even though it predicted higher sputtering yields [25]. A more recent analytical expression for $s_n(\varepsilon)$ was developed by Matsunami et al [27]:

$$s_n(\varepsilon) = \frac{3.441\sqrt{\varepsilon}\ln(\varepsilon + 2.718)}{1 + 6.35\sqrt{\varepsilon} + \varepsilon(-1.708 + 6.882\sqrt{\varepsilon})} \quad (21)$$

Sigmund's theory can not be directly applied to calculate sputtering yields at low ion energies. In this energy range sputtering takes place by the knock-on process rather than through production of a collision cascade. However, we have calculated sputtering yields at low energies using Sigmund's formula to compare with yields predicted by theoretical formulas provided by other researchers. For this calculation, we have used values of $s_n(\varepsilon)$ expressed by eq. (21).

To determine sputtering yields more accurately at low ion energies, both Bodhansky [28] and Yamamura et al (henceforth referred to as YMI) [29] proposed semi-empirical correction factors to Sigmund's formula given in eq. (17).

The correction factor suggested by Bodhansky is [28]:

$$\left(\frac{R_p}{R}\right)\left[1 - \left(\frac{E_{th}}{E}\right)^{2/3}\right]\left[1 - \left(\frac{E_{th}}{E}\right)\right]^2 \quad (22)$$

where R_p/R is depends only on the mass ratio M_2/M_1 and E_{th} is the threshold energy of the specific ion-target combination. These two functions are expressed as:

$$\frac{R_p}{R} = \frac{1}{0.4\left(\frac{M_2}{M_1}\right) + 1} \quad (23)$$

and

$$E_{th} = 8U_o\left(\frac{M_1}{M_2}\right)^{2/5} \quad (24)$$

The correction factor proposed by YMI is given by [29]:

31

$$Q\frac{1}{[1+0.35U_o s_e(\varepsilon)]}\left[1-\left(\frac{E_{th}}{E}\right)^{0.5}\right]^{2.8} \qquad (25)$$

Here Q is a constant which depends only on the target material and E_{th} is the threshold energy which is written as [27]:

$$E_{th} = U_o\left[1.9 + 3.8\left(\frac{M_2}{M_1}\right)^{-1} + 0.134\left(\frac{M_2}{M_1}\right)^{1.24}\right] \qquad (26)$$

The reduced Lindhard inelastic stopping cross-section $s_e(\varepsilon)$ is given by [30,31]:

$$s_e(\varepsilon) = \frac{0.079(M_1 + M_2)^{3/2}}{M_1^{3/2} M_2^{1/2}} \frac{Z_1^{2/3} Z_2^{1/2}}{(Z_1^{2/3} + Z_2^{2/3})^{3/4}} \varepsilon^{1/2} \qquad (27)$$

Bodhansky recommended the following formula to describe α [28]:

$$\alpha = 0.3\left(\frac{M_2}{M_1}\right)^{2/3} \qquad (28)$$

whereas the expression proposed for α by Matsunami et al [31] is:

$$\alpha = 0.08 + 0.164\left(\frac{M_2}{M_1}\right)^{0.4} + 0.0145\left(\frac{M_2}{M_1}\right)^{1.29} \qquad (29)$$

The sputtering yields of molybdenum by xenon ions calculated by using the three formulations are shown in Fig. 13. The values of the parameters used in these calculations are given in Table 1. The values of α are nearly identical in all three formulations. Hence, the changes in the shape of the theoretical yield-energy curves are due to eqs. (22) and (25) only. As

32
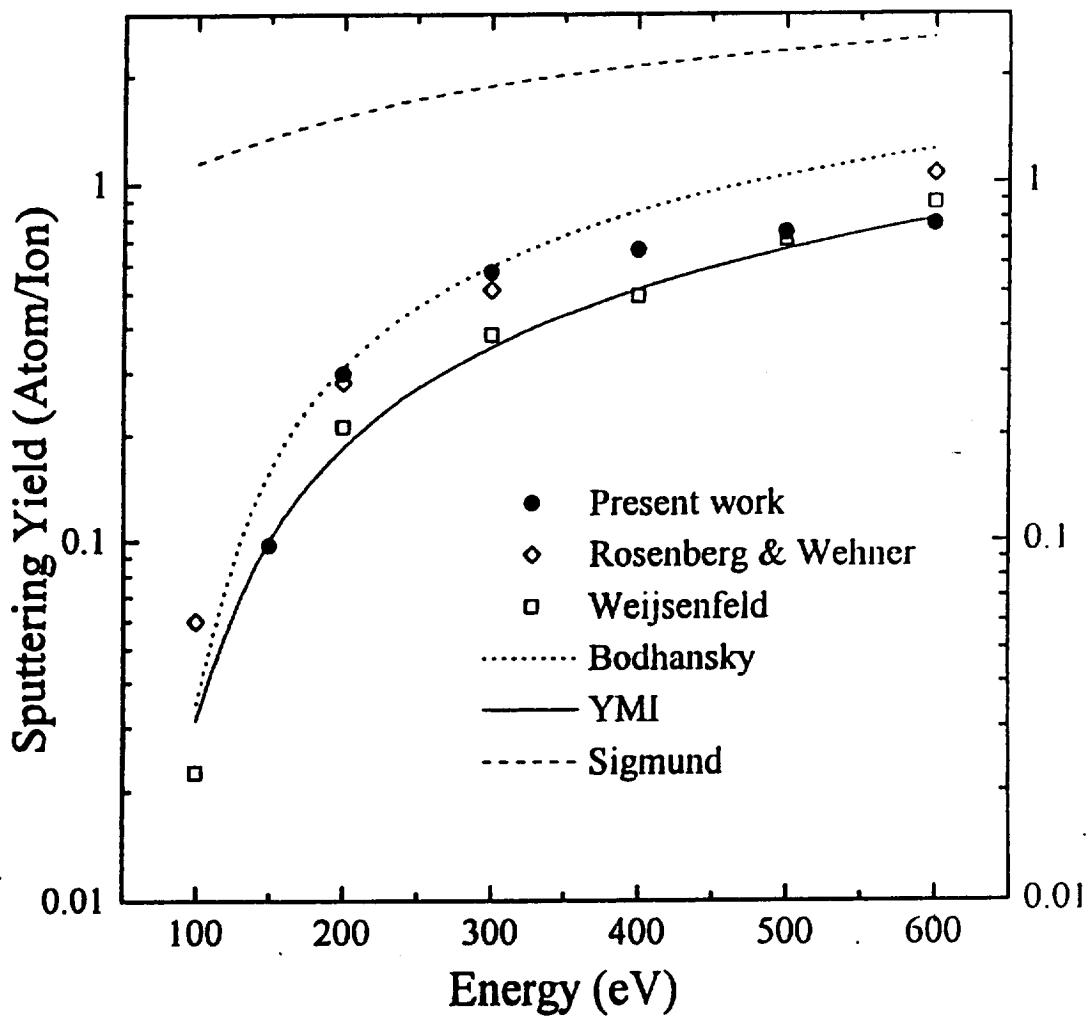
Fig.13. Comparison of theoretical sputtering yield with experimental data

Table 1. Values of parameters used in the theoretical calculations

Parameter	Bodhansky's Formulations	YMI Formulation
α	0.24	0.23
Q		0.84 [31]
(R_p/R)	0.77	
U	6.82 eV	6.82 eV [32]
E_{th}	61.8 eV	48.9 eV

expected, the yields obtained using Sigmund's formula are high. Both Bodhansky's and YMI's formulations predict the sputtering data reasonably well given the uncertainty in the sputtering data themselves. Between 200 and 600 eV, sputtering yields predicted by Bodhansky is about 55 percent higher than those predicted by YMI, whereas at 100 eV the two values are nearly same. However, both theories provide the same shape in the yield-energy curves as can be seen from Fig. 14, where the two curves are normalized at 600 eV.

Although these formulations provide a reasonable agreement with the measured sputtering yields, it should be noted that they both use very high threshold energy, E_{th}. Most measurements of sputtering threshold energies have indicated values which are twice the sublimation energy of the target or higher [33]. However, several studies have indicated values that fall below those of twice the sublimation energy [11,13]. Hence, these formulations need to be modified with the use of more realistic threshold energy values.

4.6. Conclusions

Sputtering yields of Mo by xenon ions in the 150 to 600 eV energy range were measured using a SNMS. The SNMS spectra were obtained at an angle of incidence of 50^0. They were converted to sputtering yields for perpendicular incidence by normalizing SNMS spectral data at 500 eV with the yield measured by Rutherford backscattering spectrometry. The values of sputtering yields obtained in this manner are in the range of those measured by other researchers
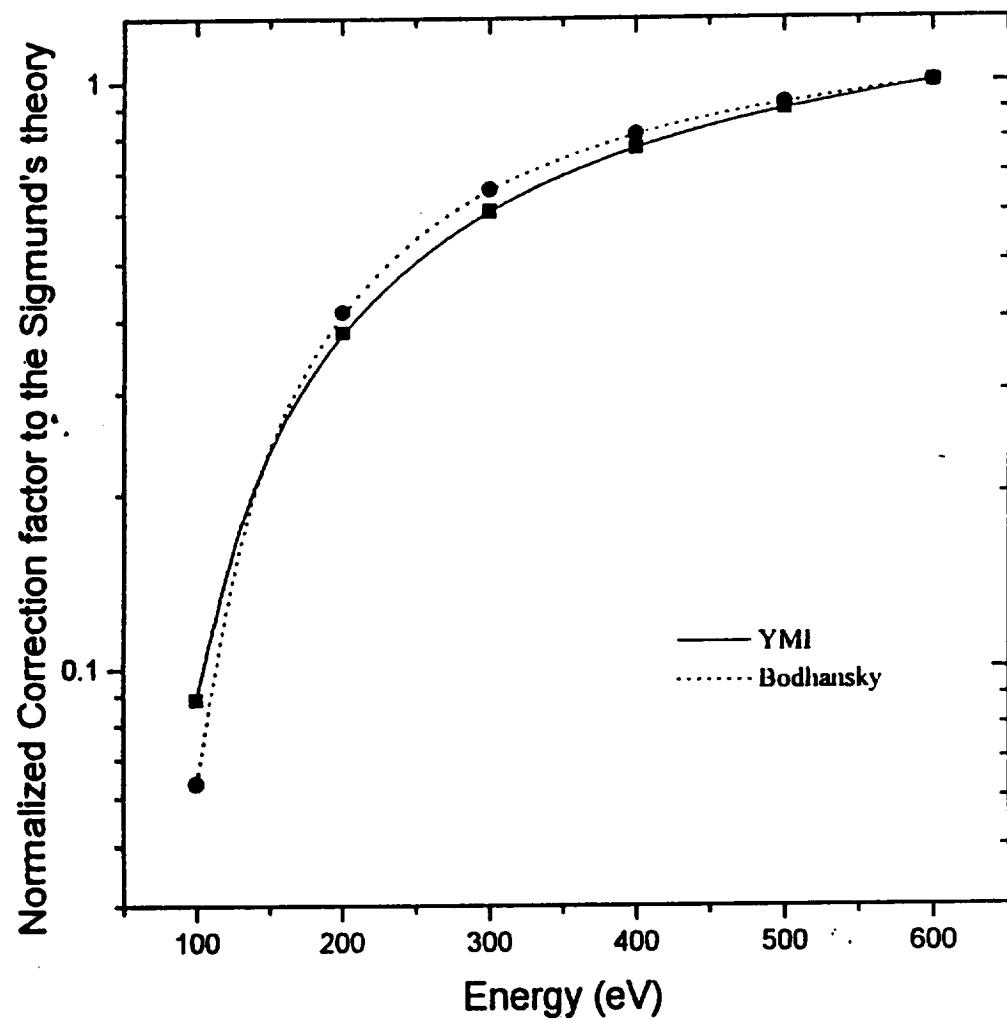
Fig.14. Normalized theoretical yields using Bodhansky and YMI formulations

even though RBS studies revealed that the peak of the sputtered material distribution shifted from 45^0 at 500 eV primary ion energy to 60^0 at 200 eV primary ion energy. The shape of the yield-energy curve is observed to have a smaller slope at energies above 300 eV than reported previously.

Sputtering yields were calculated by using formulations provided by Sigmund, Bodhansky, and YMI. The two later formulations are applicable at low ion energies. They are semi-empirical in nature and extensions of the method outlined by Sigmund. The yields calculated from these two methods agree well with the measured values in spite of the fact that both formulations use threshold energy values much higher than those observed experimentally. Significantly higher sputtering yields were obtained by using Sigmund's equations.

5. PREFERENTIAL SPUTTERING OF HEAVY ISOTOPES AT LOW INCIDENT ION ENERGIES

5.1 Introduction

When a solid surface is bombarded by energetic particles, emission of atoms, molecules, electrons, and photons from the target surface is observed. The sputtered atoms and molecules are ejected as neutrals and ions (both positive and negative) and also, in excited states. The sputtering of multicomponent materials results, at least in initial phases, in a nonstoichiometric composition of the sputtered particles. Specifically, lighter particles have been observed to be sputtered preferentially over heavier components except at large emission angles [34-39]. Hence, the eroded target surface becomes gradually enriched in the heavier component as the sputtering is continued. After prolonged bombardment, usually less than thousand seconds at keV incident particle energies, a steady state is reached with the composition of the emitted flux being identical to the bulk composition.

The emission of neutral atoms and icns in sputtering is of considerable interest both from basic and applied point of view. These include the fundamental physics of the sputtering process itself, geo-cosmology, thin film deposition and secondary ion mass spectrometry. However, the study of preferential sputtering in alloys and compounds is complicated by the existence of chemical forces between components of the target materials. The analysis becomes simpler when elements containing isotopes are sputtered. In this case, kinematic effects due to isotopic mass differences play a significant role in the preferential emission of one isotope over the other.

Several experiments have been conducted to determine isotopic enrichment at very low fluences [37-41]. Experimental investigations on preferential sputtering from elemental targets have revealed that the enrichment also depends on the emission angle [34-39] and energy of the sputtered particles [42,43]. Moreover, the enrichment has been found to be dependent on the impact energy at low incident ion energies [43]. An enrichment of light isotopes in the sputtered flux was observed in all these experiments at small emission angles. In one experiment, an enrichment of heavy isotopes was observed in the initial stages of sputtering at high incident ion energy [44], but this result is generally discounted [40] as this was not observed in any other investigation involving high impact energy .

We observed experimental evidence of enrichment of heavy isotopes in the sputtered flux of secondary ions at a comparatively small emission angle (40° to the surface normal) at low incident ion energies and also, of the gradual change from heavy to light isotope enrichment with increasing incident ion energy. This type of behavior was predicted over a decade ago from a computer simulation in situations where the incident ion had a significantly higher mass compared to that of the target atom [45], but it has not been observed experimentally until now.

5.2   Experimental procedure

In our experiment, we have used xenon ions (mass 131.3 u) to bombard a polycrystalline copper target (isotopic masses 63 u and 65 u) with energies between 100 eV to 1.5 keV. The isotopic enrichment of secondary ions was measured by a quadrupole mass spectrometer. For this study, copper was selected as a target because its two isotopes are in a mass range where very little interference was expected from the background gas molecules. Moreover, the two isotopic masses of copper are separated by two units and hence, interference from the formation of hydrides of copper was also minimized.

At low incident ion energies, yields of secondary ions are significantly reduced. Moreover, the aperture of the mass spectrometer intercepts only a small amount of secondary ions sputtered from the sample. In our experiment, xenon ions impinged on the target surface at 50° angle to the surface normal. This arrangement was chosen because at this incident angle the sputtering yields are higher compared to normal incidence. The spectrometer entrance aperture was perpendicular to the direction of the primary ion beam. Since the secondary ion intensities were significantly reduced at low primary ion energies, the ion optics parameters of the spectrometers were optimized to obtain maximum signal intensities. The width of copper peaks were 0.4 u at FWHM.

The beam current remained essentially constant from 150 eV to 1.5 keV at 0.235 μA. At 100 eV, the beam current was reduced to 0.22 μA. Data were acquired at an operational pressure of 1×10^{-6} Torr.

The target was 6.35 mm in diameter and 6 mm thick with 99.9% purity. It was mounted on a XYZθ manipulator for precise positioning within the vacuum chamber. The target was first

cleaned with acetone and distilled water and subsequently, sputter cleaned for 30 minutes using a 2.5 keV rastered ion beam to remove surface impurities. The rastered area was approximately 4 mm x 4 mm in size. The material removed from the target surface during this process is estimated to be 6 nm using a beam fluence of 1.8×10^{16} ions/cm^2. The sputter cleaning process leaves the target surface slightly mass-altered, but this should not have a significant effect on the isotopic enrichment at low incident ion energies [42,43]. The fluence was not large enough in our experiment to reach the steady state conditions. Secondary ions were collected immediately after the sputter cleaning process with the ion beam focused at the center of the cleaned area. Data for each run were acquired with a fluence of 7×10^{15} ions/cm^2.

5.3   Results and Discussion

The change of the $^{63}Cu^+/^{65}Cu^+$ isotope ratio, normalized to the natural abundance ratio of these two isotopes, is shown in Fig.15 as a function of xenon ion energy . The normalized isotope ratio measured is known as the enrichment factor. It is clear from this figure that the secondary ions are enriched in heavy isotopes at low energies. The enrichment of heavy isotopes is gradually reduced with increasing primary ion energy. Beyond 700 eV, the secondary ions are observed to be enriched in light isotopes. The maximum enrichment factor of heavy isotopes is 0.795 at 100 eV. The enrichment of light isotopes is observed to remain nearly constant with energy with an enrichment factor of 1.009.

In analyzing isotopic sputtering, the analytical treatment developed by Sigmund and co-workers is often used [46,47]. It deals with two component sputtering at high primary ion energies where the sputtered particles are assumed to originate in the collision cascade induced by the incident ion [24]. This theory predicts, in the limit of low fluence, an initial enrichment of light isotopes in the sputtered flux. At high primary ion energies, measured enrichments of light isotopes generally agree with those predicted from this theory. Since, energy and momentum are randomized in a collision cascade, no dependence of isotopic enrichment on the mass and energy of the primary ions, emission angle, and energy of the sputtered particles are obtained from this analytical treatment.
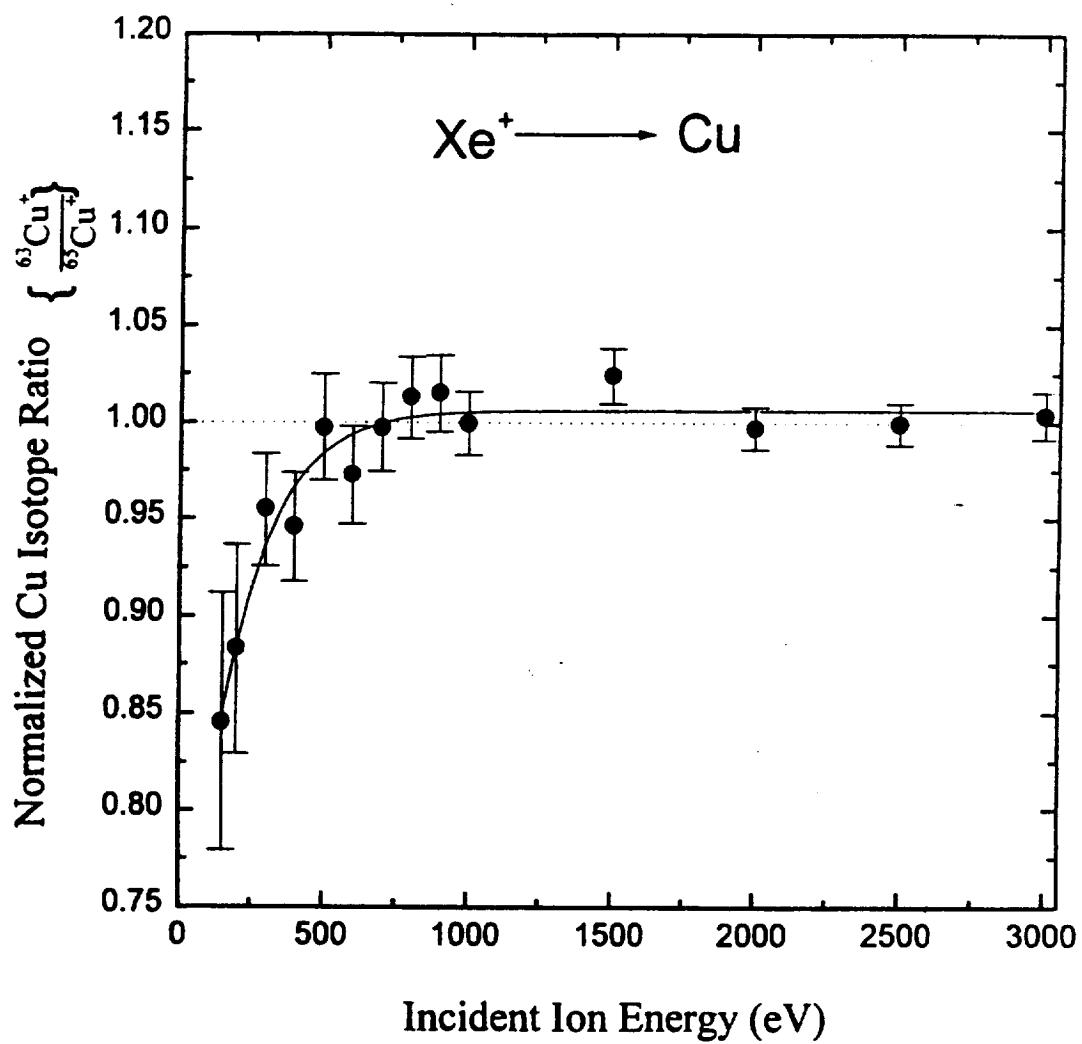
Fig.15. Change of $^{63}Cu^+/^{65}Cu^+$ isotope ratio as a function of incident ion energy

Sputtering of isotopic targets have also been studied through computer simulations. The simulation using a multiple interaction, molecular dynamics model demonstrated the variation of isotopic enrichment with the emission angle [48]. Computer simulations have also been performed with the TRIM computer code which uses a Monte Carlo method. This simulation further indicated that an enrichment of heavy isotopes is possible at low incident ion energies when the mass of the incident ion is significantly higher than the mass of the target atom [45].

The data presented in Fig. 15 can be qualitatively explained by considering the energy transfer between two atoms in a binary collision. In the collision of an ion of mass M_1, possessing kinetic energy E_1, with the target atom of mass M_2, the energy transferred to the target atom T, is given by

$$ T = \frac{4 M_1 M_2}{(M_1 + M_2)^2} E_1 \sin^2 \theta / 2 $$

$$ = \gamma(M_1, M_2) E_1 \sin^2 \theta / 2 \tag{30} $$

where $\gamma(M_1, M_2)$ is the energy transfer factor, and θ is the scattering angle of the ion in the center of mass system. For isotopes of copper sputtered by xenon, the values of γ are 0.876 for ^{63}Cu and 0.886 for ^{65}Cu. At low incident ion energies, the collision kinematics of a single collision or first few collisions near the surface will likely dominate the emission process. The single-collision or few-collisions occurring are generally not sufficient to produce energy randomization as in the linear cascade regime. Hence, in the low-energy regime, the energy transferred in binary collisions play a larger role in the particle emission process. Since, $\gamma(^{65}Cu) > \gamma(^{63}Cu)$, ^{65}Cu atoms have higher than average probability to receive more energy than ^{63}Cu atoms when xenon ions have collisions with copper atoms near the surface and hence, more $^{65}Cu^+$ are expected in the secondary ion flux at low incident ion energies.

With higher incident ion energies, the bombarding ion penetration into the target is deeper and collision cascades are expected to be more fully developed. The cross section for energy transfer in elastic scattering increases with decreasing mass of the struck particle. Therefore, light isotopes have higher than average probability of being hit, and lower than

average probability of loosing energy after being set in motion [46]. So the sputtering yields of $^{63}Cu^+$ is higher than those of $^{65}Cu^+$ at higher primary ion energies.

From the argument presented in the previous paragraphs, the enrichment of heavy isotopes is expected to be higher at lower ion energies when the mass of the incident ion is significantly higher than the mass of the target atom. With increasing primary ion energy, an increasing amount of the light isotope is likely to be sputtered until at some point, the sputtered flux is enriched in light isotopes.

These explanations are supported by an experiment where low-energy (40-440 eV) argon ions have been used to sputter copper and molybdenum [43]. The value of γ for the Ar-^{63}Cu pair is 0.95 while, for the Ar-^{65}Cu pair, it is 0.943. The corresponding values of γ for Ar-^{92}Mo and Ar-^{100}Mo pairs are 0.844 and 0.816 respectively. In both cases, γ (^{63}Cu) > γ (^{65}Cu) and γ (^{92}Mo) > γ (^{100}Mo). Hence, in the sputtering of copper and molybdenum by low-energy argon ions, the sputtered particle flux is likely to be enriched in light isotopes which was observed experimentally.

5.4   Conclusions

An experimental investigation in isotopic enrichment of secondary ions at low incident ion energies and at moderate fluence levels has been conducted. Copper was sputtered by xenon ions at energies ranging from 150 eV to 1.5 keV. The secondary ions were measured by a quadrupole mass spectrometer. The secondary ions were observed to be enriched in the heavy isotope at low ion energies. The proportion of heavy isotopes in the sputtered secondary ion flux was found to decrease with increasing primary ion energy from 150 to 700 eV. Beyond 700 eV, light isotopes were sputtered preferentially. The light isotope enrichment factor was observed to remain constant at 1.009 at higher incident ion energies.

42

6. REFERENCES

1.. F. M. Curran and L. W. Callahan, " The NASA on-board propulsion program." AIAA-2379 (1995).

2. J. R. Brophy, J. E. Polk and V. K. Rawlin, "Ion engine service life validation by analysis and testing," AIAA-96-2715 (1996).

3. X. Peng, D. Keefer, and W. M. Ruyten, "Plasma particle simulation of electrostatic ion thrusters," Journal of Propulsion and Power, 8, 361 (1992).

4. V. J. Friedly, "Hollow cathode operation at high discharge currents," NASA CR 185238 (1990).

5. J. R. Beattie and J. N. Matossian, "Mercury ion thruster technology," NASA CR 174974 (1989).

6. M. J. Patterson, V. K. Rawlin, J. S. Sovey, M. J. Kussmaul and J. Parks, "2.3 kW ion thruster wear test," AIAA-95-2516 (1995).

7. V. K. Rawlin, " Internal erosion rates of a 10-kW xenon ion thruster," AIAA-88-2912 (1988).

8. D. Rosenberg and G. K. Wehner, "Sputtering yields for low-energy He+, Kr+, and Xe+ ion bombardment," J. Appl. Phys. 33, 1842 (1962).

9. C. H. Weijsenfeld, A. Hoogendoorm, and M. Koedam, " Sputtering of polycrystalline metals by inert gas ions of low-energy (100-1000 eV)", Physica, 27, 763 (1961).

10. R. V. Stuart and G. K. Wehner, "Sputtering yields at very low bombarding ion energies", J. Appl. Phys. 33, 2345 (1962).

11. N. D. Morgulis and V. D. Tischenko, " The investigation of cathode sputtering in the near threshold region," Soviet Phys. - JETP, 3, 52 (1956).

12. A. K. Handoo and P. K. Ray, "Sputtering yield of chromium by argon and xenon ions with energies from 50 to 500 eV," Appl. Phys. A54, 92 (1992).

13. A. K. Handoo and P. K. Ray, "Sputtering of cobalt and chromium by argon and xenon ions near threshold energy region," Can. J. Phys. 71, 155 (1993).

14. G. Kiriakidis, C. E. Christodoulides, G. Carter and J. S. Colligon, "An RBS technique for

measurement of the erosion of ion implanted films," Appl. Phys. **19**, 191 (1979).

15. H. L. Bay, J. Bohdansky, W. O. Hofer and J. Roth, "Angular distribution and differential yields for low-energy light-ion irradiation of polycrystalline nickel and tungsten" Appl. Phys. **21**, 327 (1980).

16. N. P. Tognetti, R. P. Webb, C. E. Christodoulides, D. G. Armour and G. Carter, "Ion bombardment induced interface mixing in the Ag-Si system," Nucl. Instr. Meth. **182/183**, 107 (1981).

17. H. F. Winters and E. Taglauer, "Sputtering of chemisorbed nitrogen from single crystal planes of tungsten and molybdenum", Phys. Rev. **B35**, 2174 (1987).

18. L. C. Feldman and J. W. Mayer, Fundamentals of Surface and Thin Film Analysis, North-Holland, New York (1986), p. 50.

19. T. Okutani, M. Shikata, S. Ichimura and R. Shimizu, " Angular distribution of Si atoms sputtered by keV Ar^+ ions", J. Appl. Phys. **51**, 2884 (1980).

20. G. K. Wehner and D. Rosenberg, " Angular distribution of sputtered material", J. Appl. Phys. **31**, 177 (1960).

21. P. C. Zalm, "Energy dependence of the sputtering yield of silicon bombarded with neon, argon, krypton and xenon ions," J. Appl. Phys. **54**, 2660 (1983).

22. H. Tsuge and S. Esho, "Angular distribution of sputtered atoms from polycrystalline metal targets" J. Appl. Phys. **52**, 4391 (1981).

23. H. Oechsner, H. Schoof and E. Stumpe, "Sputtering of Ta_2O_5 by Ar^+ ions at energies below 1 keV", Surf. Sci. **76**, 343 (1978).

24. P. Sigmund, "Theory of sputtering: sputtering yield of amorphous and polycrystalline targets", Phys. Rev. **184**, 383 (1969).

25. P. Sigmund, in Sputtering by Particle Bombardment I, ed. R. Behrisch, Springer-Verlag, Berlin, (1981), chapter 2.

26. J. Lindhard, V. Nielsen, and M. Scharff, Dan. Vid. Selsk. Mat. Medd. **36**, No 10. (1968).

27. N. Matsunami, Y. Yamamuura, Y. Itakawa, N. Itoh, Y. Kazumata, S. Miyagawa, K. Morita, and R. Shimizu, "A semiempirical formula for the energy dependence of the sputtering yield" Rad. Eff. Lett. **57**, 15 (1980).

28. J. Bodhansky, "A universal relation for the sputtering yield of monatomic solids at normal

ion incidence", Nucl. Instr. Meth. Phys. Res. **B2**, 587 (1984).

29. Y. Yamamuura, N. Matsunami, and N. Itoh, "Theoretical studies on an empirical formula for sputtering yield at normal incidence", Rad. Eff. **71**, 65 (1983).

30. J. Lindhard, M. Scharff, and H. E. Schiott, Mat.-Fys.Medd.Danske vid.Selsk. **33**, No.14 (1963).

31. N. Matsunami, Y. Yamamuura, Y. Itakawa, N. Itoh, Y. Kazumata, S. Miyagawa, K. Morita, R. Shimizu, and H. Tawara, "Energy dependence of the ion-induced sputtering yields of monatomic solids", At. Data Nucl. Data Tables, **31**, 1 (1984).

32. C. Kittel, Introduction to Solid State Physics, John Wiley, New York , (1976), p. 74.

33. M. A. Mantenieks, "Sputtering Threshold Energies of Heavy Ions", IEPC-97-187 (1997).

34. G.K.Wehner, "Isotope enrichment in sputter deposits", "Appl Phys. Lett. **30**, 185 (1977).

35. R. R. Olson, M. E. King, and G. K. Wehner, "Mass effects on angular distribution of sputtered atoms," J. Appl. Phys. **50**, 3677 (1979).

36. W. A. Russell, D. A. Papanastrassiou and T. A. Tombrello, "The fractionation of Ca isotopes by sputtering", Rad. Eff. **52**, 41 (1980).

37. H. Gnaser and H. Oechsner, "Preferential sputtering of isotopes: Fluence and emission-angle dependence," Phys. Rev. Lett. **63**, 2673 (1989).

38. H. Gnaser and H. Oechsner, " Isotopic mass effects in sputtering: Dependence on fluence and emission angle," Nucl. Instr. Meth. Phys. Res. **B48**, 544 (1990).

39. D. L. Weathers, S. J. Spicklemire, T. A. Tombrello, I. D. Hutcheon, and H. Gnaser, "Isotopic fractionation in the sputtering of ^{92}Mo-^{100}Mo targets," Nucl. Instr. Meth. Phys. Res. **B73**, 135 (1993).

40. H. Gnaser and I. D. Hutcheon, "Preferential emission of lighter isotopes in the initial stage of sputtering," Surf. Sci. **195**, 499 (1988).

41. L. M. Baumel, M. R. Weller, R. A. Weller, and T. A. Tombrello, "Isotopic composition of boron secondary ions as a function of ion-beam fluence," Nucl. Instr. Meth. Phys. Res. **B34**, 427 (1988).

42. N. Shimizu and S. R. Hart, "Isotope fractionation in secondary ion mass spectrometry," J. Appl. Phys. **53**, 1303 (1982).

43. W. Bieck, H. Gnaser, and H. Oechsner, "Isotopic mass effects in low-energy sputtering of

45

copper and molybdenum," Nucl. Instr. Meth. Phys. Res. **B101**, 335 (1995).

44. J. Okano, T. Ochiai, and H. Nishimura, "Ion-beam-induced isotope composition changes in metal surfaces and recoil implantation," Appl. Surf. Sci. **22/23**, 72 (1985).

45. W. Eckstein and J. P. Biersack, "Computer simulation of two-component target sputtering," Appl. Phys. **A37**, 95 (1985).

46. P. Sigmund, "Preferential sputtering from isotopic mixtures and alloys of near-neighbor elements," Nucl. Instr. Meth. Phys. Res. **B18**, 375 (1987).

47. P. Sigmund, A. Oliva, and G. Falcone, "Sputtering of multicomponent materials: elements of a theory", Nucl. Instr. Meth. Phys. Res. **194**, 541 (1982).

48. M. H. Shapiro, P. K. Haff, T. A. Tombrello and D. E. Harrison, "Simulation of isotopic mass effects in sputtering," Nucl. Instr. Meth. Phys. Res. **B12**, 137 (1985).

REPORT DOCUMENTATION PAGE

Public reporting burden for this collection of information is estimated to average 1 hour per response, including the time for reviewing instructions, searching existing data sources, gathering and maintaining the data needed, and completing and reviewing the collection of information. Send comments regarding this burden estimate or any other aspect of this collection of information, including suggestions for reducing this burden, to Washington Headquarters Services, Directorate for Information Operations and Reports, 1215 Jefferson Davis Highway, Suite 1204, Arlington, VA 22202-4302, and to the Office of Management and Budget, Paperwork Reduction Project (0704-0188), Washington, DC 20503.

1. AGENCY USE ONLY (Leave blank)	2. REPORT DATE	3. REPORT TYPE AND DATES COVERED
	June 1999	Contractor Report

4. TITLE AND SUBTITLE

Low-Energy Sputtering Research

5. FUNDING NUMBERS

WU–632–1B–1B–00
NAG3–1388

6. AUTHOR(S)

P.K. Ray and J. Shutthanandan

7. PERFORMING ORGANIZATION NAME(S) AND ADDRESS(ES)

Tuskegee University
Mechanical Engineering Department
Tuskegee, Alabama 36088

8. PERFORMING ORGANIZATION REPORT NUMBER

E–11725

9. SPONSORING/MONITORING AGENCY NAME(S) AND ADDRESS(ES)

National Aeronautics and Space Administration
Washington, DC 20546–0001

10. SPONSORING/MONITORING AGENCY REPORT NUMBER

NASA CR—1999-209161

11. SUPPLEMENTARY NOTES

Project Manager, Maris Mantenieks, Power and On-Board Propulsion Technology Division, NASA Glenn Research Center, organization code 5430, (440) 977–7460.

12a. DISTRIBUTION/AVAILABILITY STATEMENT

Unclassified - Unlimited
Subject Categories: 20 and 72   Distribution: Nonstandard

This publication is available from the NASA Center for AeroSpace Information, (301) 621–0390.

12b. DISTRIBUTION CODE

13. ABSTRACT (Maximum 200 words)

An experimental study is described to measure low-energy (less than 600 eV) sputtering yields of molybdenum with xenon ions using Rutherford backscattering spectroscopy (RBS) and secondary neutral mass spectroscopy (SNMS). An ion gun was used to generate the ion beam. The ion current density at the target surface was approximately 30 μA/cm^2. For RBS measurements, the sputtered material was collected on a thin aluminum strip which was mounted on a semi-circular collector plate. The target was bombarded with 200 and 500 eV xenon ions at normal incidence. The differential sputtering yields were measured using the RBS method with 1 MeV helium ions. The differential yields were fitted with a cosine fitting function and integrated with respect to the solid angle to provide the total sputtering yields. The sputtering yields obtained using the RBS method are in reasonable agreement with those measured by other researchers using different techniques. For the SNMS measurements, 150 to 600 eV xenon ions were used at 50° angle of incidence. The SNMS spectra were converted to sputtering yields for perpendicular incidence by normalizing SNMS spectral data at 500 eV with the yield measured by Rutherford backscattering spectrometry. Sputtering yields as well as the shape of the yield-energy curve obtained in this manner are in reasonable agreement with those measured by other researchers using different techniques. Sputtering yields calculated by using two semi-spherical formulations agree reasonably well with measured data. The isotopic composition of secondary ions were measured by bombarding copper with xenon ions at energies ranging from 100 eV to 1.5 keV. The secondary ion flux was found to be enriched in heavy isotopes at low incident ion energies. The heavy isotope enrichment was observed to decrease with increasing impact energy. Beyond 700 eV, light isotopes were sputtered preferentially with the enrichment remaining nearly constant.

14. SUBJECT TERMS

Electronic propulsion; Ion thrusters; Sputtering

15. NUMBER OF PAGES

56

16. PRICE CODE

A04

17. SECURITY CLASSIFICATION OF REPORT	18. SECURITY CLASSIFICATION OF THIS PAGE	19. SECURITY CLASSIFICATION OF ABSTRACT	20. LIMITATION OF ABSTRACT
Unclassified	Unclassified	Unclassified	

NSN 7540-01-280-5500